ADVANCED FUNCTIONAL MATERIALS
www.afm-journal.de

Polymorphism-Dependent Emission for Di(p-methoxylphenyl)dibenzofulvene and Analogues: Optical Waveguide/Amplified Spontaneous Emission Behaviors

Xinggui Gu, Jingjing Yao, Guanxin Zhang, Yongli Yan, Chuang Zhang, Qian Peng, Qing Liao, Yishi Wu, Zhenzhen Xu, Yongsheng Zhao, Hongbing Fu, and Deqing Zhang**

The synthesis and optical investigations of di(p-methoxylphenyl)dibenzofulvene (1) and its analogues 2, 3, 4, 5, 6, and 7 with different lengths of alkoxyl chains are presented. All of these molecules exhibit emission in the solid state. The following interesting properties are reported for compound 1: 1) the solid-state fluorescence of 1 is dependent on the polymorphism forms; the two crystalline forms 1a and 1b are strongly blue- and yellow-green-emissive, whereas the amorphous solid is weakly fluorescent with orange emission; 2) on the basis of crystal-structural analysis, the intermolecular interactions will restrict the internal rotations, leading to fluorescence enhancement for the two crystalline forms 1a and 1b; however, the difference in emission color between 1a and 1b is ascribed to the molecular conformational alteration; 3) the solid-state fluorescence of 1 can be tuned by heating and cooling as well as grinding. Importantly, microrods of 1a and 1b exhibit outstanding optical waveguide behaviors. Moreover, amplified spontaneous emission for 1b and multimode-lasing behavior for 1a are presented. Besides the studies of compound 1, the crystal structures and solid-state fluorescence behaviors of 2, 3, 4, 5, 6, and 7 are also described.

1. Introduction

Organic materials that exhibit strong emission in the solid states have received increasing attentions in recent years because of their potential applications in optical devices and optoelectronic devices such as optical waveguides,[1,2] optically pumped lasers[3] and light-emitting diodes.[4] However, many luminophores that are highly luminescent in diluted solution become weakly or even non-emissive in the aggregations and solid states. Such fluorescence quenching is usually attributed to intermolecular interactions leading to formation of detrimental species such as excimers and exciplexes.[5] Various approaches have been explored to inhibit the intermolecular interactions and hence yield emissive organic materials.[6] In recent years, Tang and other groups have reported several types of organic molecules which show abnormal fluorescent behaviors; they are weakly or non-emissive in solution, but they become strongly emissive upon formation of aggregation states and in the solid states.[7] For instance, siloles,[8] tetraphenylethylenes[9] and diphenyldibenzofulvenes[10] were found to show strong emission after aggregation. Such aggregation-induced-(enhanced) emission is mainly ascribed to inhibition of internal rotations.[7–11] Moreover, it is interesting to note that the emission features of a few organic molecules are dependent on the aggregation states; they emits faintly in the amorphous states but strongly in the crystalline states.[10,12]

For the practical applications in optoelectronic devices as well as sensors[13–15] and memories,[16,17] organic emissive materials whose emission intensities and colors can be tuned are highly desirable. The most common approach is to modify the respective chemical structures and hence tune the emission properties of luminophores. It is still challenging to tune the fluorescence behaviors of organic molecules in the solid states. There are a few reported examples of fluorescence tuning for organic molecules in the solid states upon heating, grinding and exposure to chemical vapor.[18–21] In particular, mechanochromic fluorescence has been observed for derivatives of oligo(*p*-phenylene vinylene) with cyano groups and long alkyl chains,[19] pyrene and anthracene based liquid crystals[20] and coordination complexes of copper, gold and platinum.[21]

In this paper, we want to report thorough studies of di(p-methoxylphenyl)dibenzofulvene (**1**, **Scheme 1**) and its analogues with alkxoyl groups of different lengths (**2**, **3**, **4**, **5**, **6** and **7**) in

Prof. D. Q. Zhang, Dr. G. X. Zhang, X. G. Gu, Dr. Q. Peng, J. J. Yao
Beijing National Laboratory for Molecular Sciences
Key Laboratory of Organic Solid
Institute of Chemistry
Chinese Academy of Sciences
Beijing 100190, P. R. China
E-mail: dqzhang@iccas.ac.cn; gxzhang@iccas.ac.cn
Dr. Y. L. Yan, C. Zhang, Dr. Q. Liao, Dr. Y. S. Wu, Z. Z. Xu, Prof. Y. S. Zhao, Prof. H. B. Fu
Beijing National Laboratory for Molecular Sciences
Key Laboratory of Photochemistry
Institute of Chemistry
Chinese Academy of Sciences
Beijing 100190, P. R. China

DOI: 10.1002/adfm.201201482

ADVANCED FUNCTIONAL MATERIALS
www.afm-journal.de

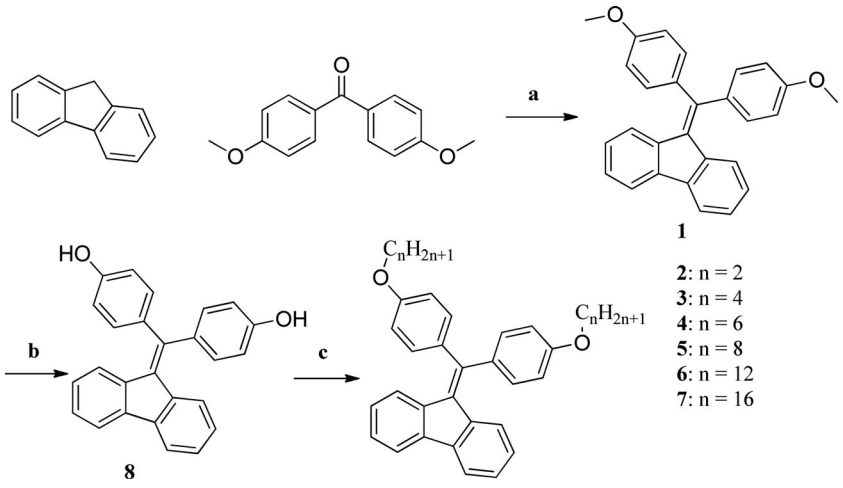

Scheme 1. The synthetic approach for compounds **1**, **2**, **3**, **4**, **5**, **6** and **7**. Reagents and conditions: a) n-BuLi, THF, –78 °C; b) BBr_3, CH_2Cl_2; c) K_2CO_3, DMF, $C_nH_{2n+1}Br$, 60 °C.

terms of polymorphism-dependent emission in the solid state, interesting optical waveguide and amplified spontaneous emission behaviors. The studies intend to examine 1) whether polymorphism-dependent emission is a general phenomenon for alkoxyl substituted diphenyldibenzofulvenes; 2) how the alkyl chains influence the emission behaviors; 3) whether the strongly emissive diphenyldibenzofulvenes in the solid states can be used as optical waveguides and even exhibit amplified spontaneous emission behaviors. The results reveal that 1) compounds **1** and **2** with two methoxyl and two ethoxyl groups, respectively, possess two stable crystalline forms which exhibit different color emissions with high quantum efficiencies. In comparison, their corresponding amorphous forms are weakly emissive; 2) the emission behaviors of diphenyldibenzofulvenes in the solid state can also be tuned by varying the alkoxyl chains; 3) microrods of **1** exhibit interesting optical waveguide and amplified spontaneous emission behavior.

2. Results and Discussions

2.1. Synthesis and Characterization

The synthesis of compounds **1**, **2**, **3**, **4**, **5**, **6** and **7** is shown in Scheme 1. Coupling of fluorene and bis(4-methoxyphenyl)methanone in the presence of n-BuLi led to compound **1** in 30% yield.[10a] Demethoxylation of **1** and further reaction with the respective alkylbromides in the presence of K_2CO_3 yielded compounds **2**, **3**, **4**, **5**, **6** and **7** in acceptable yields. The chemical structures of **1**, **2**, **3**, **4**, **5**, **6** and **7** were confirmed by NMR and MS data (see Experimental Section).

As reported for diphenyldibenzofulvenes,[10] compounds **1**, **2**, **3**, **4**, **5**, **6** and **7** are almost non-emissive in good solvents such as THF. However, they become strongly emissive after further introducing poor solvents such as water. As an example, Figure S1 in the Supporting Information shows the fluorescence spectra of **1** in THF and THF/water mixture with 95% fraction of water. Obviously, the fluorescence intensity increased upon addition of water because of the formation aggregates of **1** as reported early.[10] In fact, such fluorescence enhancement can be detected with naked eyes as illustrated in the inset of Figure S1 where the photos of two solutions of **1** in THF and THF/water (5:95, v/v) under UV light illumination were displayed.

2.2. Polymorphism-Dependent Emission for 1

Interestingly, two kinds of crystals of **1** were obtained by slow evaporation of the solution of **1** in dichloromethane/petroleum ether (1:4, v/v). **Figure 1**A and Figure 1B show photos of two kinds of crystals under daylight and their CLSM (confocal laser scanning microscope) images together with those of the amorphous one which will be discussed below. One is colorless with blue emission (referred to as **1a**), and the other is yellow with yellow-green emission (referred to as **1b**).

The absorption and fluorescence spectra of **1a** and **1b** were measured (see Figures S2 (Supporting Information) and 1C). **1a** exhibited no absorption above 450 nm, whereas **1b** absorbed in the region of 450–500 nm. Compared to the emission of **1a** with λ_{max} = 466 nm, the fluorescence spectrum of **1b** was red-shifted to 518 nm. The solid state fluorescence quantum efficiencies of **1a** and **1b** were measured to be 0.95 and 0.62, respectively, thus both **1a** and **1b** were highly emissive in the solid state. Additionally, the solid state fluorescence decay was also measured for **1a** and **1b** (see Figure S3, Supporting Information), and accordingly their average fluorescence lifetimes ($<\tau>$) were estimated to be 4.96 ns and 1.89 ns, respectively (see **Table 1**). In addition, the respective radiative rate constants (k_r) and the non-radiative rate constants (k_{nr}) were also deduced and listed in Table 1. For **1a** and **1b**, the respective k_r is clearly larger than k_{nr}, being consistent with the fact that both **1a** and **1b** are strongly emissive. These results reveal that **1a** and **1b**,

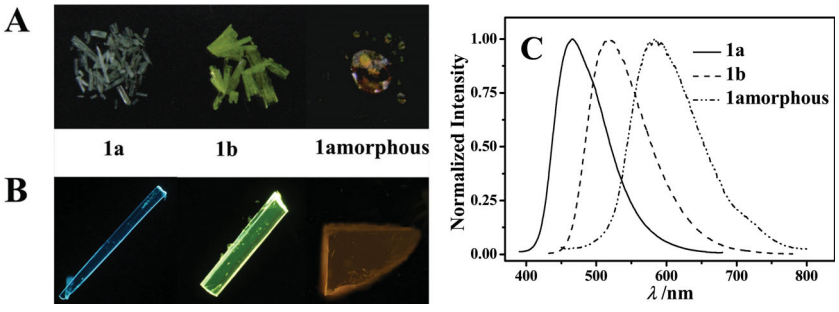

Figure 1. A,B) Daylight photos (A) and CLSM images (B) of **1**: blue emission crystal (**1a**), yellow-green emission crystal (**1b**) and amorphous solid (**1amorphous**). C) The respective fluorescence spectra of **1a**, **1b**, and **1amorphous**.

DOI: 10.1002/adfm.201201482

Table 1. The photophysical properties of **1a**, **1b**, and **1amorphous**.

Compound	Absorption λ_{max} [nm]	Fluorescence λ_{max} [nm]	$<\tau>^{a)}$ [ns]	$\Phi_f^{b)}$	$k_r^{c)}$ [$\times 10^8$ s^{-1}]	$k_{nr}^{c)}$ [$\times 10^8$ s^{-1}]
1a	398	466	4.96	0.95	1.92	0.10
1b	400	518	1.89	0.62	3.28	2.01
1amorphous	450	583	0.30	0.05	1.67	1.66

[a)] An apparent decay time constant $<\tau>$ was determined by using the relation

$$<\tau>=\sum_{i=1}^{n} a_i \times \tau_i \Big/ \sum_{i=1}^{n} a_i \times \tau_i \ (n = 2 \sim 3),$$

where τ_i and a_i, respectively, represent the individual exponential decay time constant and the corresponding preexponential factor;[22] [b)] Φ_f is measured by calibrated integrating sphere; [c)] The radiative rate constant $k_r = \Phi_f/<\tau>$; the non-radiative rate constant $k_{nr} = 1/<\tau> - k_r$.

two crystalline forms of **1**, exhibit different emission behaviors, which may be attributed to either different molecular conformations of **1** or different intermolecular interactions in two crystals.

Crystal structures of **1a** and **1b** were determined, and the respective crystallographic data were listed in Table S1, Supporting Information. Crystal **1a** belongs to monoclinic system with one molecule in the asymmetric unit, and crystal **1b** belongs to orthorhombic system with two molecules in the asymmetric unit. **Figure 2** shows the molecular structures of **1a** and **1b**. Their bonding lengths and angles are in normal region. The torsion angles of C13-C14-C15-C16 and C13-C14-C22-C28 in **1a** are 74.40° and 57.95°, respectively. In comparison, the corresponding torsion angles in **1b** are 65.43° and 44.83°, respectively. Obviously, the fluorene ring in **1b** is relatively more coplanar with the two benzene rings. Thus, it is expected that the pi-electron conjugation degree in **1b** is higher than that in **1a**. Accordingly, such molecular conformational alteration from **1a** to **1b** may attribute to their differences in absorption and emission spectra. Theoretical calculations also support this assumption as to be discussed below.

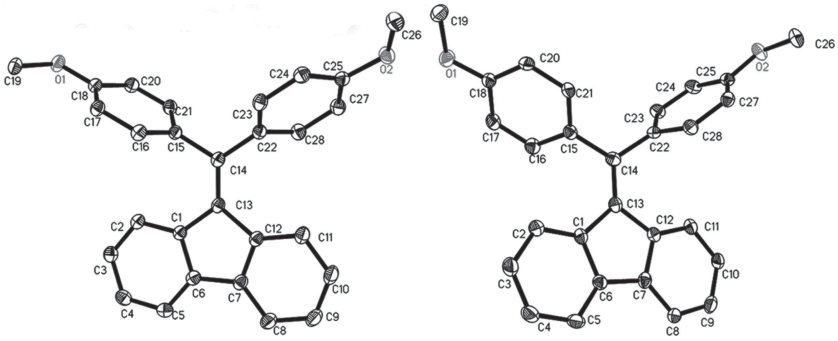

Figure 2. Molecular structures of **1a** (left) and **1b** (right); the hydrogen atoms have been omitted for clarity.

Figure S4 (Supporting Information) shows the intermolecular arrangements of **1a** and **1b**. Molecules of **1a** are arranged as *zigzag* chains along the a-axis, whereas molecules of **1b** are stacked as layers along the c-axis. The twisted conformations of **1a** and **1b** rule out specific strong intermolecular interactions (such as π–π stacking or H/J-aggregates) in their crystals. In fact, fluorene and benzene rings of neighboring molecules are not parallel and no pi-pi interactions exist in crystals of both **1a** and **1b**. Thus, the formation of intermolecular H- or J-aggregates within crystals of **1a** and **1b** can be eliminated.[23] However, multiple interatomic short contacts (C…O: 3.18 Å, O…H: 2.71 Å, 2.65 Å in **1a**; C…C: 3.39 Å, O…H: 2.77 Å, 2.76 Å in **1b**) and C-H…pi interactions (2.77 Å, 2.86 Å in **1a**; 2.80 Å, 2.81 Å, 2.84 Å, 2.85 Å, 2.86 Å, 2.88 Å, 2.89 Å in **1b**) exist in crystals of **1** (see Figure S5, Supporting Information). These intermolecular weak interactions will fix the molecular conformations of **1a** and **1b** in the solid states, thus inhibit the internal rotations and block the non-radioactive relaxation, according to previous studies.[8–12] Furthermore, compared to those in **1b** the interatomic contacts in **1a** are shorter; thus, intermolecular interactions in **1a** are stronger, and accordingly the molecular conformation of **1a** in the solid state will be fixed more completely. This is consistent with the fact that **1a** shows higher emission quantum yield in the solid state. The following conclusions may be drawn from the crystal structures of **1a** and **1b**: 1) the multiple intermolecular interactions will inhibit the internal rotations and thus turn-on the fluorescence of **1a** and **1b**; 2) the fact that the pi-electron conjugation degree within **1b** is higher than that in **1a** is attributed to the red-shift of the emission maxima of **1b** compared to that of **1a**.

Theoretical calculations (QM/MM)[24] of compound **1** lead to two stable conformations. One shows torsion angles of C13-C14-C15-C16 and C13-C14-C22-C28 are 68.88° and 57.84°, being close to those of **1a** (see above); torsion angles of C13-C14-C15-C16 and C13-C14-C22-C28 are 64.68° and 45.82° for another conformation, which are close to those of **1b**. The absorption maxima of two conformations were calculated to be 374 nm and 385 nm, and their emission maxima were 454 nm and 539 nm (see Table S2, Supporting Information). These calculation results manifest that the red-shift of the emission maximum observed for **1b** compared to **1a** is mainly caused by the molecular conformational change.

Alternatively, quickly cooling the molten crystals of either **1a** or **1b** with liquid nitrogen led to the amorphous form of **1** for which only a broad XRD diffraction signal was detected (see Figure S6, Supporting Information). Injection of the ethanol solution of **1** into water also led to the amorphous form based on the XRD diffraction profile (see Figure S6, Supporting Information). Compared to those of **1a** and **1b**, the absorption spectrum of the amorphous form was red-shifted as depicted

in Figure S2, Supporting Information. Interestingly, the amorphous form exhibited orange emission with maximum at 583 nm, which was red-shifted by 117 nm and 65 nm compared to those **1a** and **1b**, respectively (see Figure 1C). However, the fluorescence quantum efficiency of this amorphous form was found to be 0.05, much lower than those of **1a** and **1b** (see Table 1). Also, the average fluorescence lifetime of this amorphous form was measured to be 0.30 ns, being shorter than those of **1a** and **1b** (see Table 1). Compared to those of **1a**, k_r decreased slightly and k_{nr} was enhanced by more than 15 times for the amorphous form (see Table 1). It is not likely to deduce the exact molecular conformation of **1** in the amorphous form, but we speculate that the red-shifted weak emission from the amorphous form may be due to 1) molecules of **1** are loosely packed in the amorphous form, and as a result internal rotations within **1** cannot be inhibited leading to weak emissions as reported previously;[10] 2) molecules in the amorphous form have more volume. Thus, molecules may become more planar with higher conjugation degree and accordingly the emission becomes red-shifted.

In short, two crystals and one amorphous form were found for **1**. Of interest is the fact that they exhibit different emission behaviors; two crystals are strongly emissive with different emission maxima and the amorphous form shows weak orange emission. It should be noted that this is abnormal feature as crystallization usually decreases the emission efficiency and amorphization leads to fluorescence enhancement for normal fluorophores. As to be discussed below the three forms can be interconverted by heating and grinding and thus the solid state emission can be tuned.

2.3. Tuning the Solid-State Fluorescence of 1 by Heating and Grinding

Apart from the melting point at 151 °C, a broad endothermic peak was detected around 135 °C for **1a** (see the DSC curve of **1a** in Figure S7, Supporting Information). Such DSC data manifest that there is a phase transition around 135 °C for **1a**. In fact, blue-emissive crystals of **1a** were transformed into yellow-green-emissive crystals after heating at 135 °C for 15 min. in air as depicted in **Figure 3**. XRD analysis shows that the resulting yellow-green-emissive crystals possess good crystallinity and exactly the same crystallographic parameters as for **1b**. Moreover, the emission spectrum of these yellow-green-emissive crystals is almost the same as that of **1b**. Therefore, heating at 135 °C led to the successful crystal-to-crystal transformation of **1a** into **1b**. Sequential cooling of the yellow-green-emissive crystals that were generated by heating **1a** could not lead to re-generation of **1a**; this may indicate that **1b** is more thermodynamically stable than **1a**. Alternatively, melting of either **1a** or **1b** occurred after heating over 151 °C. Fast cooling of the melting state with liquid nitrogen yielded the weakly-emissive amorphous form as mentioned above. However, slow cooling of the melting state led to yellow-green-emissive **1b** as shown in Figure S8 (Supporting Information), where the fluorescence spectra of three forms of **1** generated via heating and cooling were displayed. In short, **1b** can be formed by either heating of **1a** at 135 °C or cooling of the melting state slowly, and the fluorescence is tuned accordingly.

Interestingly, grinding of fine crystals of **1a** via agate mortar led to yellow solids as shown in the inset of **Figure 4**A. The yellow solids after grinding of **1a** exhibit a few diffraction signals with weak intensities (rather than broad diffraction signal) compared to **1a** in the form of fine crystals (see Figure 4B).

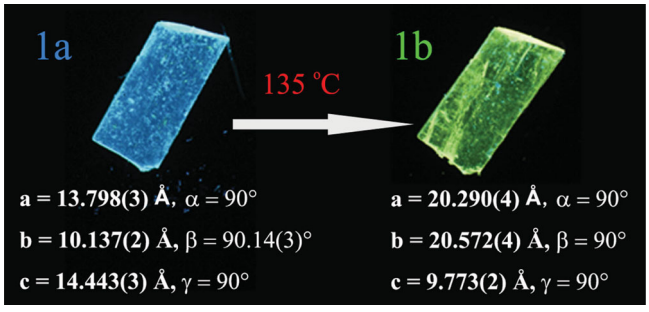

Figure 3. The PL image of crystal-to-crystal transformation of **1a** into **1b** by heating at 135 °C.

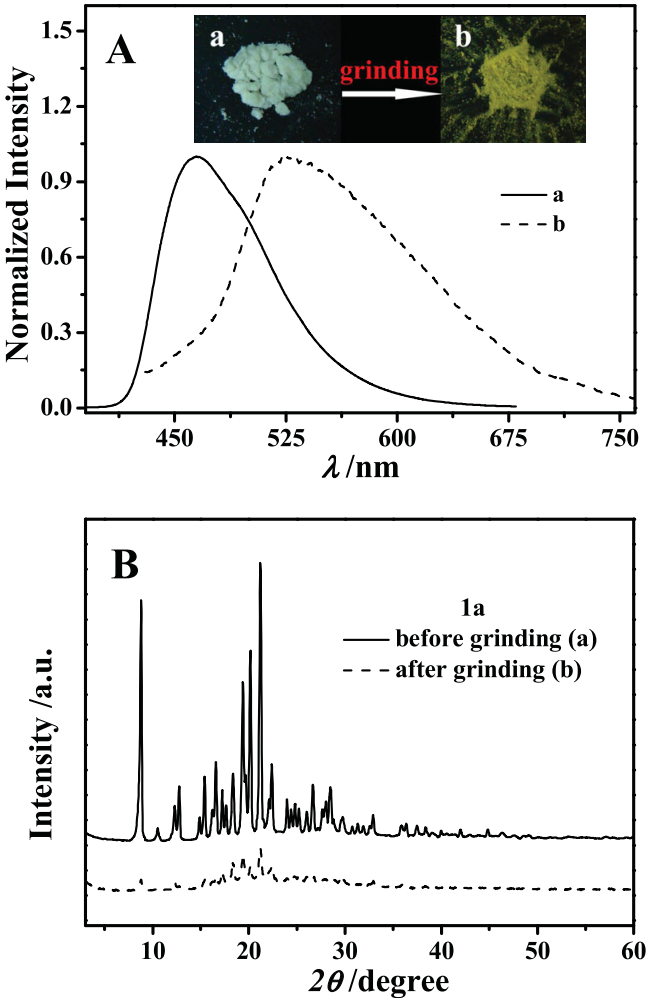

Figure 4. A) The fluorescence spectra of **1a** before (a) and after (b) grinding; the inset shows the respective photos under daylight. B) The XRD of **1a** before and after grinding.

Adv. Funct. Mater. **2012**,
DOI: 10.1002/adfm.201201482

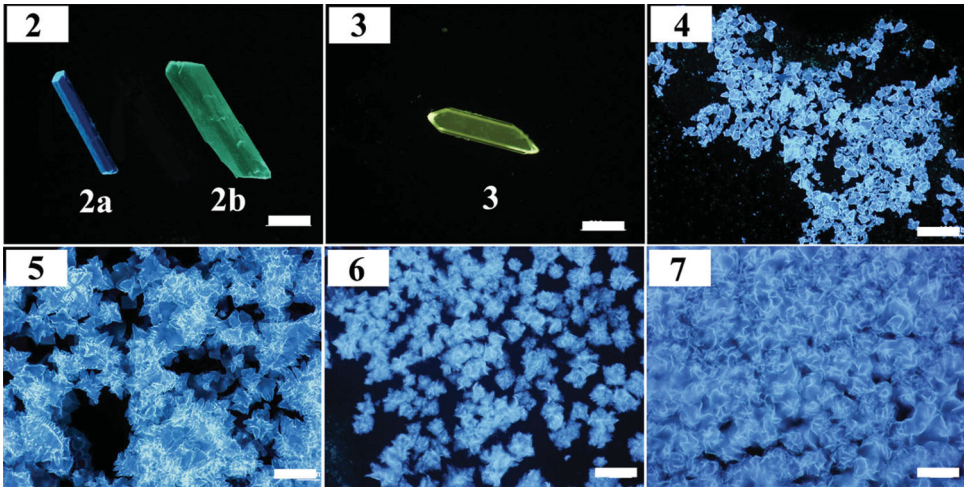

Figure 5. CLSM images of crystals of **2** (**2a** and **2b**) and **3**, microcrystalline powders of **4**, **5**, **6** and **7** from crystallization; the scale bar is 100 µm.

Thus, after grinding the crystallinity is significantly reduced and accompanied with obvious color change. Moreover, such yellow solids show rather weak emission with λ_{max} = 525 nm as shown in Figure 4A. The emission maximum lies between those of **1b** and the amorphous form of **1** (see Figure 1C). Such emission spectral variation is probably due to the transformation of **1a** into **1b** and further partial conversion into the amorphous form after grinding. Similarly, grinding of fine crystals of **1b** also led to emission intensity reduction and red-shift.

2.4. The Influence of the Alkoxyl Chains on the Fluorescent Behavior of Diphenyldibenzofulvenes

With the end to examine the influence of alkyl chains on the solid state fluorescence behaviors of diphenyldibenzofulvene compounds, longer alkyl chains than methyl were linked to diphenyldibenzofulvene framework leading to analogues of **1**, compounds **2**, **3**, **4**, **5**, **6** and **7** (see Scheme 1). During our studies, Tang and coworkers reported the diphenyldibenzofulvene with two *n*-propoxyl groups, and two crystal forms as well as the amorphous state with different emission behaviors were described.[25] Interestingly, compound **2** also exists three morphology forms, the blue- (**2a**) and yellow-green-emissive (**2b**) crystals (see the CLSM images in **Figure 5**) as well as the weakly emissive-amorphous solid. Both the blue-emissive (λ_{max} = 448 nm, see Figure S3, Supporting Information) and the yellow-green-emissive (λ_{max} = 499 nm) crystals were found to be highly fluorescent with quantum yields of 0.72 and 0.58, respectively (see Table S3, Supporting Information). In comparison, the fluorescence quantum yield of the amorphous solid (the emission maximum λ_{max} = 578 nm) was measured to be 0.05 (see Table S3, Supporting Information). Additionally, the average fluorescence lifetimes of the blue-/yellow-green-emissive crystallines and the amorphous solid were estimated based on the respective fluorescence decays as listed in Table S3, Supporting Information; these fluorescence lifetimes are consistent with the fact that the blue-/yellow-green-emissive crystals are strongly emissive while the amorphous solid is weakly fluorescent.

The crystal structures of the blue- and yellow-green-emissive crystalline forms of **2** were determined. **Figure 6** depicts the respective molecular structures of the blue- and yellow-green-emissive crystalline forms of **2**. As for compound **1**, the two structures for the crystalline forms of **2** are conformational isomers. Being different from **1** the two isomers (**2a** and **2b**) are structurally symmetrical around the ethylene bonds. The torsion angle C7-C8-C9-C14 in **2a** is 83.35°, respectively. In comparison, this in **2b** forms is 77.48°. Obviously, the fluorene ring in **2b** is relatively more coplanar with the benzene ring (C9-C10-C11-C12-C13-C14). Thus, it is expected that the pi-electron conjugation degree in **2b** is higher than that in **2a**. Accordingly, such molecular conformational alteration from **2a** to **2b** may attribute to their differences in absorption and emission spectra. The multiple interatomic short contacts (C…H: 2.83 Å, O…H: 2.47 Å in **2a**; O…H: 2.74 Å in **2b**) and C-H…pi interactions (2.86 Å, 2.87 Å, 2.90 Å, 2.92 Å, 2.93 Å, 2.94 Å, 2.95 Å in **2a**; 2.91 Å, 2.92 Å, 2.93 Å, 2.96 Å, 2.98 Å in **2b**) exist in crystals of **2**, (see Figure S9, Supporting Information) but

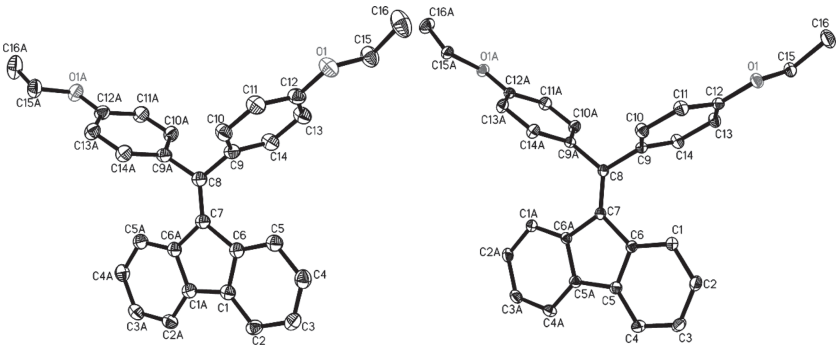

Figure 6. Molecular structures of **2a** (left) and **2b** (right); the hydrogen atoms have been omitted for clarity.

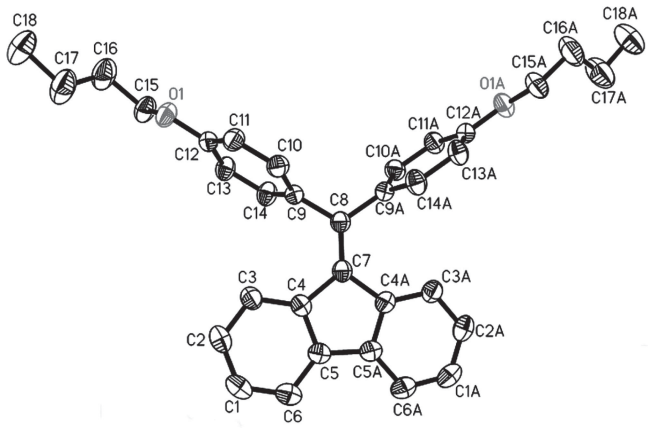

Figure 7. Molecular structure of **3**; the hydrogen atoms have been omitted for clarity.

intermolecular pi-pi interactions can be neglected because of the large separation among aromatic rings. Therefore, the red-shift of the emission maximum of **2b** compared to that of **2a** should be attributed to the molecular conformational difference between them as for **1**.

Attachment of two butoxyl groups to diphenyldibenzofulvene framework leads to compound **3**. Several crystallization conditions were tested, and only one crystalline form was yielded for **3** (see the CLSM image in Figure 5). Photophysical investigations manifest that crystals of **3** are highly emissive with fluorescence quantum yield of 0.54 (see Table S3, Supporting Information). The emission maximum ($\lambda_{max.}$ = 522 nm) was more red-shifted compared to those of **1b** and **2b** (see Figure S3, Supporting Information). As shown in **Figure 7**, the molecular structure of **3** is symmetrical around the ethylene bond. The torsion angle C7-C8-C9-C14 in **3** is 74.44°, respectively. Again, the intermolecular pi-pi interactions do not exist within crystal structure of **3**, but interatomic short contacts O…H (2.67Å) and C-H…pi interactions (2.94Å, 2.98Å) (see Figure S11, Supporting Information) further restrict the internal rotations which will accordingly lead to fluorescence enhancement.

Compounds **4**, **5**, **6** and **7** entail longer alkoxyl chains. Their single crystals of good qualities were not obtained though many efforts; as a result their crystal structures were not determined. However, the respective microcrystallines were yielded (see the CLSM images in Figure 5). As depicted in Figure S12 (Supporting Information) several sharp diffraction peaks were detected for **4**, **5**, **6** and **7**. Table S3 (Supporting Information) summarizes the fluorescence quantum yields and lifetimes of the respective microcrystallines of **4**, **5**, **6** and **7**. Obviously, microcrystallines of **4**, **5**, **6** and **7** are highly emissive with the emission maximum around 450 nm (see Figure S3, Supporting Information). As for compounds **1**, **2** and **3** the corresponding amorphous forms of **4**, **5**, **6** and **7** could be prepared similarly by melting the respective microcrystallines, followed by quick cooling with liquid nitrogen. The amorphous forms of **4**, **5**, **6** and **7** were found to be weakly fluorescent around 570 nm; but those of **6** and **7** were unstable and easily transformed into the corresponding crystallines.

As detailed above compounds **1** and **2** with shorter (than *n*-butoxyl) alkoxyl chains possess two crystalline forms with different emission colors, whereas for **3** with *n*-butoxyl and longer (than *n*-butoxyl) alkoxyl chains only one crystalline form was yielded. The blue-emissive forms of **1** and **2** as well as **4**, **5**, **6** and **7** are highly fluorescent in the crystalline forms; interestingly, their emission maxima were slightly dependent on the lengths of alkoxyl chains (see Figure S3, Supporting Information). Similarly, the yellow-green-emissive forms of **1** and **2** as well as **3** are also highly fluorescent; the emission of **3** is slightly more red-shifted compared to the yellow-green-emissive forms of **1** and **2** (see Figures 1C and S3). It was reported previously that alkyl chains could influence the intermolecular pi-pi interactions of conjugated molecules and as a result their emission behaviors in the solid states were tuned.[26] For **1**, **2**, **3**, **4**, **5**, **6** and **7**, however, alkoxyl chains do not affect the intermolecular pi-pi interactions of diphenyldibenzofulvene framework significantly based on the crystal structural analysis of **1a**, **1b**, **2a**, **2b** and **3**. It is probable that alkoxyl chains within **1**, **2**, **3**, **4**, **5**, **6** and **7** may affect the molecular conformations and thus the pi-conjugation degree leading to variation of the emission maxima for short alkoxyl chains.

2.5. The Waveguide Behavior of Microrods of 1

Figure 8A and Figure 8B show the photoluminescence (PL) images of microrods of **1a** and **1b**, respectively. The microrods of both **1a** and **1b** exhibit bright luminescence spots at the two rod-ends and relatively weaker emission from the rod-bodies, which is a characteristic of optical waveguides. These microrods can absorb the excitation light and propagates the PL emission toward the respective rod-ends. Almost all of the observed microrods of **1a** and **1b** possess the waveguide behavior.

The microrods were excited with a focused laser down to the diffraction limit at different local positions along the length of the microrods. Figure 8C depicts the microarea PL microscopy images for microrods of **1a**. Interestingly, blue emission was observed from both ends of the microrods of **1a** irrespective of the excitation position. In general, the emission of light can only be observed at the local area of the excited position. The appearance of the outcoupling light at the ends of each microrod of **1a** is a typical characteristic of strong waveguide behavior. Because the waveguided light is generated from the PL, such microrods of **1a** can be classified as active waveguides based on previous reports.[1,2]

As shown in Figure 8D where the microarea PL microscopy images of microrods of **1b** are displayed, yellow-green emission was detected at the ends of microrods of **1b** upon excitation at different positions. Thus, microrods of **1b** also function as active waveguides. Furthermore, yellow-green emission was also observed after each excitation along the short-axis direction (the respective left and right sides of each excitation area). Accordingly, microrods of **1b** are able to propagate light in two dimensions.[27]

In order to gain further insight into the light waveguide behaviors within microrods of **1a** and **1b**, their spatially resolved PL spectra were measured. Figure 8E shows the collected PL spectra at the end of a single microrod of **1a** under

DOI: 10.1002/adfm.201201482

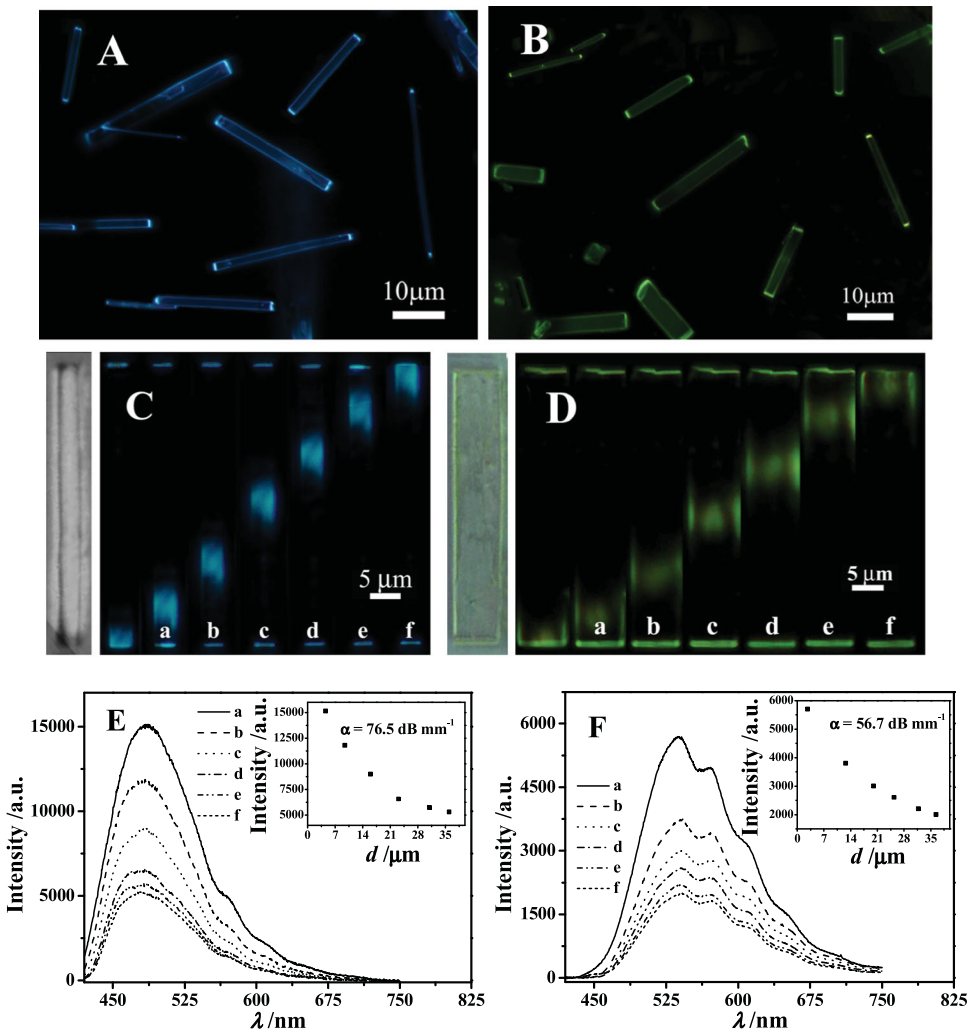

Figure 8. A,B) PL microscopy images of microrods of **1a** (A) and **1b** (B) deposited on a glass wafer. C) (for **1a**) and D) (for **1b**) Bright-field images (on the left side of each PL image) and microarea PL images by exciting identical microcrystals of **1a** and **1b** at six different positions, respectively. Both samples were excited with a focused UV laser (351 nm). E) (for **1a**) and F) (for **1b**) spatially resolved PL spectra of the emissions that are out-coupled at the tip of the microcrystals of **1a** and **1b** (curves from top to bottom: a, b, c, d, e, f); the insets show plots of the peak intensity at the respective maxima vs. the propagation distance for **1a** and **1b**.

the excitations at different positions (labeled as a, b, c, d, e and f). Obviously, the emission intensity at the microrod-ends decreases upon increasing the propagation distance. As depicted in the inset of Figure 8E, the emission intensity at 480 nm of the outcoupled light decreases almost exponentially with the propagation distance. Note that the emission intensities of the excited points do not change substantially with the position along the microrods. Thus, the inset of Figure 8E can also represent the variation of intensity ratio of incident and outcoupled light vs. the propagation distance. By fitting the data of inset of Figure 8E according to the reported procedure, the optical loss coefficient at 480 nm for microrods of **1a** was estimated to be 76.5 dB mm^{-1}.

Similarly, the PL spectra at the end of a single microrod of **1b** were measured (see Figure 8F). The emission intensities decrease obviously by prolonging the light propagation distance. By fitting the variation of emission intensity at 538 nm vs. the propagation distance shown in the inset of Figure 8F, the optical loss coefficient for microrods of **1b** was estimated to be 56.7 dB mm^{-1}.

The observed optical loss for microrods of **1a** and **1b** may come from the following sources based on previous studies:[1,2] 1) self-absorption, 2) the effect of glass substrate and 3) Rayleigh scattering due to defects within microrods, which will lead to the local variation of refractive index along the microrods. On the basis of the fact that the corresponding absorption and fluorescence spectral overlap is small for **1a** and **1b** in their crystalline states (see Figure S13, Supporting Information), self-absorption may not contribute largely to the optical loss during the light propagation. This is indeed in agreement with the observation that the emission spectral profiles at the ends of either **1a** or **1b** keep almost unaltered upon increasing the propagation distance (see Figures 8E and 8F).

In addition, the microarea PL microscopy images and the PL spectra at the end of a single microrod upon excitation at different positions were also measured for the respective

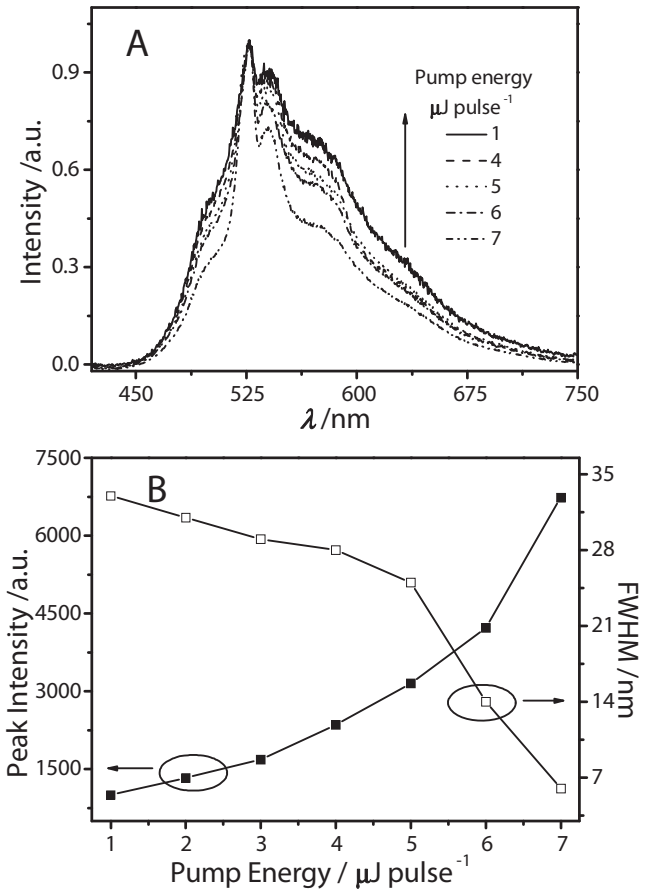

Figure 9. A) PL spectra of crystal **1b** as a function of the pump laser energy. B) Variation of the peak intensity and FWHM of emission spectra with the pump laser energy.

microrods of **2a**, **2b** and **3** (see Figures S14 and S15, Supporting Information). These results manifest that microrods of **2a**, **2b** and **3** also exhibit active waveguide behaviors. Moreover, the corresponding optical loss coefficients for microrods of **2a**, **2b** and **3** were also estimated and those of **2a** and **3** were relatively small.[28]

2.6. The Amplified Spontaneous Emission Behavior of Microrods of 1

As discussed above, the microrods of **1a** and **1b** show outstanding waveguide property. In general, waveguided propagation of the emission is thought to be one prerequisite for lasing and amplified spontaneous emission (ASE).[3,29] The PL spectra of the microrod of **1b** were collected at the excitation position as a function of the pump laser energy (see **Figure 9**A). Figure 9B shows the plot of the peak intensity and full width at half maximum (FWHM) of emission spectra versus the pump laser energy. By increasing the pump energy, a gain-narrowed peak rises out of the broad emission spectrum as depicted in Figure 9A. The FWHM of the emission spectra changes from 33 nm at 1.0 μJ pulse^{-1} to 6 nm at 7.0 μJ pulse^{-1}. The relationship between the peak intensity and the pump energy is nonlinear. Such behavior is characterized as ASE according to previous reports.[29] The slope changes at 5.3 μJ pulse^{-1}, which can be regarded as the threshold value of ASE. However, the modes of lasing were not observed at room temperature.

However, the ASE phenomenon was not observed around 470 nm for **1a** (see Figure S16, Supporting Information) upon increasing the pump laser energy. Interestingly, the multimode lasing was generated between 520 nm and 550 nm upon exposure to pump laser (10 μJ pulse^{-1}) (see Figure S16, Supporting Information). The mode spacing is ca.1.7 nm. However, such multimode lasing was not detected immediately after exposure to the pump laser. The appearance of the gain-narrowed emission signals is probably due to the partial transformation of **1a** into **1b** which shows emission in the range of 520–550 nm (see Figure 9A). As discussed above, **1a** can be transformed into **1b** upon heating, and it is anticipated that the microcrystallines of **1a** can be heated upon exposure of pump laser. Further investigations are underway.[30]

3. Conclusions

Diphenyldibenzofulvene compounds **1**, **2**, **3**, **4**, **5**, **6** and **7** with different lengths of alkoxyl chains were synthesized and investigated. All of these molecules display AIE (aggregation-induced emission) features. For compound **1**, two crystalline forms and the amorphous solid were obtained. Interestingly, the solid state fluorescence of **1** was found to be dependent on the morphology forms; the two crystalline forms were strongly blue- and yellow-green-emissive, whereas the amorphous solid was weakly fluorescent with orange emission. On the basis of crystal structural analysis, the intermolecular interaction will restrict the internal rotations leading to fluorescence enhancement for the two crystalline forms **1a** and **1b**; but, the difference in emission color between **1a** and **1b** is ascribed to the molecular conformational alteration. Crystal-to-crystal transformation was realized from **1a** to **1b** by heating at 135 °C, and the amorphous form was easily obtained by heating either **1a** or **1b** to the melting states, followed by fast cooling with liquid nitrogen. Moreover, either **1a** or **1b** can be partially transformed into the amorphous form by grinding. In these ways, the solid state fluorescence of **1** can be tuned by heating and grinding.

The influences of the alkoxyl chains on the solid state fluorescence behaviors of diphenyldibenzofulvene framework were investigated. Compound **2** with two ethoxyl chains also exists two crystalline forms which are strongly blue- and yellow-green-emissive, respectively. However, for **3**, **4**, **5**, **6** and **7** with *n*-butoxyl and longer (than *n*-butoxyl) alkoxyl chains only one emissive crystalline form was yielded. These studies manifest that alkyl chains within compounds **1**, **2**, **3**, **4**, **5**, **6** and **7** can affect the molecular conformations and thus the pi-conjugation degree leading to variation of the emission maxima.

Importantly, microrods of **1a** and **1b** as well as those of **2a**, **2b** and **3** were found to exhibit outstanding optical waveguide behaviors. Moreover, amplified spontaneous emission for **1b** and multimode-lasing behavior for **1a** were detected by increasing the pump laser energy. These results clearly reveal that diphenyldibenzofulvene compounds deserve further

DOI: 10.1002/adfm.201201482

attentions for the development of new functional materials for organic optics.

4. Experimental Section

General: All chemical materials were purchased from Alfa aesar for direct use. The water used was purified by Millipore filtration system. ^{1}H NMR and ^{13}C NMR were collected on Bruker Avance 400-MHz spectrometer. MALDI-TOF and MS were recorded with BEFLEX III spectrometer. Absorption spectra were recorded on UV-VIS-NIR spectrophotometer (UV-3600, Shimadzu spectrometer). Steady-state fluorescence spectra were recorded with Hitachi (F-4500) spectrophotometers at 25 °C. Fluorescence confocal laser scanning images were recorded with Olympus research inverted system microscope (FV1000-IX81, Tokyo, Japan) equipped with a charge couple device (CCD, Olympus DP71, Tokyo, Japan) camera; the excitation source is a Hg lamp equipped with a band-pass filter (330 ~ 380 nm). DSC analysis was carried out using a SII DSC6220 instrument at a scanning rate of 10 °C/min. All photographs were recorded on a Canon digital camera.

Crystal Structural Analysis: Crystals of **1**, **2** and **3** were grown by slow evaporation from the respective solutions: **1a** and **1b** from the dichloromethane/petroleum ether solution, **2b** from the dichloromethane/petroleum ether solution, **2a** from the dichloromethane/methanol solution, and **3** from the dichloromethane/petroleum ether or the dichloromethane/methanol solution. All single crystals data were collected on Rigaku Saturn diffractometer with CCD area detector. All calculations were performed using the SHELXL97 and crystal structure crystallographic software packages. Powder X-Ray diffraction (XRD) patterns of **4**, **5**, **6** and **7** were carried out in the reflection mode at room temperature using a 2 kW Rigaku X-ray diffraction system. Crystallographic data (excluding structure factors) for the structure(s) reported in this paper have been deposited with the Cambridge Crystallographic Data Centre as supplementary publication no. CCDC:833259, 833260, 833261, 833262, 833262.

Photophysical Studies: Quantum efficiencies of **1**, **2**, **3**, **4**, **5**, **6** and **7** in the solids states (crystals and microcrystalline powders) were recorded on FLSP 920 fluorescence spectroscopy with a calibrated integrating sphere system. Fluorescence lifetimes of **1**, **2**, **3**, **4**, **5**, **6** and **7** were measured based on the time-resolved PL experiments which were made with a regenerative amplified Ti: sapphire laser (Spectra-Physics, Spitfire) at 400 nm (150 fs pulse width, second harmonic). The PL spectra were recorded with a streak camera (C5680, Hamamatsu Photonics) attached to a polychromator (Chromex, Hamamatsu Photonics), which the temporal and spectral resolutions of the detector are ~10 ps and 2 nm, respectively. All the spectroscopic measurements were carried out at room temperature.

Optical Waveguide and ASE Measurements: To measure the microarea PL spectra of single microrod, the microrods dispersed on a glass cover-slip were excited with a UV laser (λ = 351 nm, Beamlok, Spectra-physics). The excitation laser was filtered with a band-pass filter (330–380 nm), then focused to excite the microrod with an objective (50x, N.A. = 0.80). For ASE experiments, the excitation source was delivered from an OPA (TOPAS, Spectra-physics) which is pumped by a pulsed Ti: sapphire femtosecond laser (Solstice, Spectra-physics, pulse duration 200 fs, repetition rate 1000 Hz). After passing through a narrow band filt (LD01-405, Semrock), the excitation laser was focused on the sample by the same objective and the spot size was less than 2 µm. The collected microarea PL emission were filtered by a long-pass filter (BA420), and coupled to a grating spectrometer (Acton, SP-2358) with matched ProEm: 512B EMCCD camera (Princeton Instruments).

Computational Methodology: In this work, our computational QM/MM model is established on the basis of the X-ray diffraction crystal structure. Figure S17 (Supporting Information) shows the QM/MM cluster of **1a**, where 59 molecules (3068 atoms) are included. In the same way, the clusters for **1b**, **2a**, **2b**, and **3** are set up and include 45 (2340 atoms), 21(1218 atoms), 19 (1102 atoms), 15 (1050 atoms) molecules, respectively. For all the compounds studied in the paper, the geometry optimizations are performed on the QM region while the MM region is fixed. Then the excitation energies are calculated at the optimized configurations of the ground and the excited states.

All the QM/MM calculations were carried out by the ChemShell 3.4 interface package, where QM was performed for the center molecule at DFT/TDDFT (B3LYP/SV(P)) level with Turbomole 6.3 package and the surrounding molecules were treated with the General Amber force field (GAFF) as implemented in DL-POLY package. The electrostatic embedding scheme is applied in the QM/MM calculations, namely, the MM charges were incorporated into the one-electron part of the QM Hamiltonian and the QM/MM electrostatic interactions were evaluated from the QM electrostatic potential and the MM partial charges.

Synthesis and Characterization: Compound **1** was synthesized and purified according to the reported procedures.[10a]

Compound ***8***: To a solution of **1** (3.90 g, 10 mmol) in dry dichloromethane under N_2 atmosphere at 0 °C were added of BBr_3 (25 mL, 25 mmol) in a dropwise way, after which the temperature of the solution was allowed to raise to room temperature. After being stirred overnight, HCl (25 mL, 25 mmol) were added to the solution slowly and the reaction mixture was stirred for additional 1.0 h. Then, the yellow precipitate was filtered off, which was dissolved in ethyl acetate and washed with water three times and dried with anhydrous sodium sulfate. Evaporation of solvents afforded a crude material that was purified by a silica gel column using petroleum ether/ethyl acetate (5:1 v/v) as eluent. Compound **8** was obtained as a yellow powder (3.30 g) in 91% yield. ^{1}H NMR (400 MHz, Acetonitrile-d_6, δ): 7.77 (d, 2H), 7.25 (t, 2H), 7.18 – 7.16 (m, 6H), 6.98 (t, 2H), 6.88 (d, 4H), 6.74 (d, 2H); ^{13}C NMR (100 MHz, Acetonitrile-d_6, δ): 158.4, 147.5, 140.8, 139.9, 135.7, 133.5, 132.4, 128.1, 127.2, 125.3, 120.2, 116.4; HRMS (EI) *m/z*: [M$^+$] calcd for $C_{26}H_{18}O_2$, 362.1307; found, 362.1312.

Compound **2**: To a solution of **8** (0.181 g, 0.50 mmol) in dry DMF (10 mL) under N_2 atmosphere was added K_2CO_3 (0.152 g, 1.1 mmol) and the mixture was stirred for 30 min.. Then, 1-bromoethane (0.5 mL, 6.65 mmol) was added into the mixture and the reaction solution was maintained at 50 °C for 8.0 h. After removal of DMF, the residue was dissolved in dichloromethane, and the resulting solution was washed with water three times and dried with anhydrous sodium sulfate. After purified with a silica gel column using petroleum ether/dichloromethane (5:1 v/v) as eluent, compound **2** (0.177 g, 0.43 mmol) as a white microcrystal was obtained in 85% yield. ^{1}H NMR (400 MHz, Acetone-d_6, δ): 7.80 (d, 2H), 7.25 (d, 6H), 7.01 – 6.94 (m, 6H), 6.77 (d, 2H), 4.14 – 4.09 (m, 4H), 1.43 – 1.39 (t, 6H); ^{13}C NMR (100 MHz, Acetone-d_6, δ): 160.4, 147.0, 141.0, 139.9, 136.2, 133.8, 132.3, 128.1, 127.1, 125.3, 120.1, 115.5, 64.2, 15.1; HRMS (EI) *m/z*: [M$^+$] calcd for $C_{30}H_{26}O_2$, 418.1933; found, 418.1938.

Compounds **3**, **4**, **5**, **6**, and **7** were synthesized and purified similarly as for compound **2**.

Compound **3**: Yield: 86%. ^{1}H NMR (400 MHz, Acetone-d_6, δ): 7.81 (d, 2H), 7.25 (t, 6H), 7.02 (d, 4H), 6.96 (t, 2H), 6.78 (d, 2H), 4.08 (t, 4H), 1.82 – 1.77 (m, 4H), 1.57 – 1.51 (m, 4H), 1.01 – 0.98 (t, 6H); ^{13}C NMR (100 MHz, Acetone-d_6, δ): 160.6, 147.0, 141.0, 139.9, 136.2, 133.8, 132.3, 128.1, 127.1, 125.3, 120.1, 115.5, 68.4, 32.1, 19.9, 14.1; HRMS (EI) *m/z*: [M$^+$] calcd for $C_{34}H_{34}O_2$, 474.2559; found, 474.2565.

Compound ***4***: Yield: 84%. ^{1}H NMR (400 MHz, CD_2Cl_2,δ): 7.72 (d, 2H), 7.25 – 7.21 (t, 6H), 6.97 – 6.92 (m, 6H), 6.79 (d, 2H), 4.02 (t, 4H), 1.83 – 1.78 (m, 4H), 1.54 – 1.50 (m, 4H), 1.38 – 1.37 (m, 8H), 0.93 (br, 6H); ^{13}C NMR (100 MHz, CD_2Cl_2,δ): 160.6, 146.9, 140.9, 140.1, 136.2, 133.8, 132.6, 127.9, 127.1, 125.4, 120.0, 115.4, 69.1, 32.5, 30.2, 26.7, 23.5, 14.7; HRMS (EI) *m/z*: [M$^+$] calcd. for $C_{38}H_{42}O_2$, 530.3185; found, 530.3190.

Compound ***5***: Yield: 86%. ^{1}H NMR (400 MHz, CD_2Cl_2,δ): 7.72 (d, 2H), 7.23 (t, 6H), 6.97 – 6.91 (m, 6H), 6.79 (d, 2H), 4.02 (t, 4H), 1.85 – 1.78 (m, 4H), 1.49 – 1.47 (m, 4H), 1.35 – 1.32 (m, 16H), 0.90 – 0.89 (m, 6H); ^{13}C NMR (100 MHz, CD_2Cl_2,δ): 160.6, 146.9, 140.9, 140.1, 136.2, 133.8, 132.6, 127.9, 127.1, 125.5, 120.0, 115.4, 69.1, 32.8, 30.3, 30.2, 27.0, 23.6, 14.8; HRMS (EI) *m/z*: [M$^+$] calcd for $C_{42}H_{50}O_2$, 586.3811; found, 586.3818.

Compound ***6***: Yield: 85%. ^{1}H NMR (400 MHz, CD_2Cl_2,δ): 7.72 (d, 2H), 7.23 (t, 6H), 6.97 – 6.92 (m, 6H), 6.78 (d, 2H), 4.02 (t, 4H), 1.83 – 1.80 (m, 4H), 1.51 – 1.47 (m, 4H), 1.28 (br, 32H), 0.89 – 0.87 (m, 6H); ^{13}C NMR (100 MHz, CD_2Cl_2,δ): 160.6, 146.9, 140.9, 140.1, 136.2, 133.8, 132.6, 127.9, 127.1, 125.4, 120.0, 115.4, 69.1, 49.7, 32.8, 30.5, 30.32, 30.26, 30.2, 27.0, 23.6, 14.8; HRMS (EI) *m/z*: [M$^+$] calcd for $C_{50}H_{66}O_2$, 698.5063; found, 698.5071.

Compound ***7***: Yield: 90%. ^{1}H NMR (400 MHz, CD_2Cl_2, δ): 7.72 (d, 2H), 7.25 – 7.23 (m, 6H), 6.94 – 6.92 (m, 6H), 6.79 (d, 2H), 4.02 (t, 4H), 1.83 – 1.80 (m, 4H), 1.49 (br, 4H), 1.27 (br, 52H), 0.88 – 0.86 (m, 6H); ^{13}C NMR (100 MHz, CD_2Cl_2, δ): 160.5, 146.9, 140.9, 140.1, 136.2, 133.8, 132.6, 127.9, 127.1, 125.4, 120.0, 115.4, 69.1, 32.8, 30.6, 30.33, 30.25, 30.21, 29.7, 29.5, 29.4, 29.1, 27.0, 26.7, 23.6, 14.8; HRMS (EI) *m/z*: [M$^+$] calcd for $C_{58}H_{82}O_2$, 810.6315; found, 810.6325.

Supporting Information

Supporting Information is available from the Wiley Online Library or from the author.

Acknowledgements

The present research was financially supported by Chinese Academy of Sciences, NSFC and State Key Basic Research Program. This work was also supported by the China-German Joint project (TRR61).

Received: June 2, 2012
Revised: June 30, 2012
Published online:

[1] a) L. M. Tong, R. R. Gattass, J. B. Ashcom, S. L. He, J. Y. Lou, M. Y. Shen, I. Maxwell, E. Mazur, *Nature* **2003**, *426*, 816; b) K. Takazawa, Y. Kitahama, Y. Kimura, G. Kido, *Nano Lett.* **2005**, *5*, 1293; c) X. Wang, Y. Zhou, T. Lei, N. Hu, E. Q. Chen, J. Pei, *Chem. Mater.* **2010**, *22*, 3735.

[2] a) C. Zhang, Y. S. Zhao, J. N. Yao, *Phys. Chem. Chem. Phys.* **2011**, *13*, 9060; b) Q. Liao, H. B. Fu, J. N. Yao, *Adv. Mater.* **2009**, *21*, 4153; c) J. Y. Zheng, Y. L. Yan, X. P. Wang, Y. S. Zhao, J. X. Huang, J. N. Yao, *J. Am. Chem. Soc.* **2012**, *134*, 2880; d) Y. L. Lei, Q. Liao, H. B. Fu, J. N. Yao, *J. Am. Chem. Soc.* **2010**, *132*, 1742.

[3] a) V. Bulovi , V. G. Kozlov, V. B. Khalfin, S. R. Forrest, *Science* **1998**, *279*, 553; b) X. F. Duan, Y. Huang, R. Agarwal, C. M. Lieber, *Nature* **2003**, *421*, 241; c) Y. S. Zhao, A. D. Peng, H. B. Fu, Y. Ma, J. N. Yao, *Adv. Mater.* **2008**, *20*, 1661; d) I. D. W. Samuel, G. A. Turnbull, *Chem. Rev.* **2007**, *107*, 1272.

[4] a) T. M. Figueira-Duarte, K. Müllen, *Chem. Rev.* **2011**, *111*, 7260; b) H. Aziz, Z. D. Popovic, N. X. Hu, A. M. Hor, G. Xu, *Science* **1999**, *283*, 1900; c) W. Z. Yuan, P. Lu, S. M. Chen, J. W. Y. Lam, Z. M. Wang, Y. Liu, H. S. Kwok, Y. G. Ma, B. Z. Tang, *Adv. Mater.* **2010**, *22*, 2159; d) J. H. Lee, Y. Y. Yuan, Y. J. Kang, W. L. Jia, Z. H. Lu, S. N. Wang, *Adv. Funct. Mater.* **2006**, *16*, 681; e) M. L. Tang, Z. N. Bao, *Chem. Mater.* **2011**, *23*, 446.

[5] a) R. H. Friend, R. W. Gymer, A. B. Holms, J. H. Burroughes, R. N. Marks, C. D. Taliani, D. C. Bradley, D. A. Dos Santos, J. L. Brédas, M. Lögdlund, W. R. Salaneck, *Nature* **1999**, *397*, 121; b) S. A. Jenekhe, J. A. Osaheni, *Science* **1994**, *265*, 765; c) S. W. Yin, Q. Peng, Z. Shuai, W. Fang, Y.-H. Wang, Y. Luo, *Phys. Rev. B: Condens. Matter* **2006**, *73*, 205409; d) J. B. Birks, *Photophysics of Aromatic Molecules*, Wiley, London **1970**.

[6] a) W. S. Li, T. Aida, *Chem. Rev.* **2009**, *109*, 6047; b) V. D. Halluex, J. P. Calbert, P. Brocorens, J. Cornil, J. P. Declercq, J. L. Brédas, Y. Geerts, *Adv. Funct. Mater.* **2004**, *14*, 649; c) J. Cornil, D. Beljonne, J. P. Calbert, J. L. Brédas, *Adv. Mater.* **2001**, *13*, 1053; d) Z. J. Zhao, Z. M. Wang, P. Lu, C. Y. K. Chan, D. D. Liu, J. W. Y. Lam, H. H. Y. Sung, I. D. Williams, Y. G. Ma, B. Z. Tang, *Angew. Chem. Int. Ed.* **2009**, *48*, 7608; e) G. X. Huang, B. D. Ma, J. M. Chen, Q. Peng, G. X. Zhang, Q. H. Fan, D. Q. Zhang, *Chem. Eur. J.* **2012**, *18*, 3886.

[7] a) Y. N. Hong, J. W. Y. Lam, B. Z. Tang, *Chem. Soc. Rev.* **2011**, *40*, 5361; b) Z. Y. Zhang, B. Xu, J. H. Su, L. P. Shen, Y. S. Xie, H. Tian, *Angew. Chem. Int. Ed.* **2011**, *50*, 11654; c) B. Wang, Y. C. Wang, J. L. Hua, Y. H. Jiang, J. H. Huang, S. X. Qian, H. Tian, *Chem. Eur. J.* **2011**, *17*, 2647; d) Y. H. Jiang, Y. C. Wang, J. L. Hua, J. Tang, Bo. Li, S. X. Qian, H. Tian, *Chem. Commun.* **2010**, *46*, 4689; e) Y. Y. Tam, K. M. C. Wong, V. W. Yam, *J. Am. Chem. Soc.* **2009**, *131*, 6253; f) D. Oelkrug, A. Tompert, J. Gierschner, H. J. Egelhaaf, M. Hanack, M. Hohloch, E. Steinhuber, *J. Phys. Chem. B* **1998**, *102*, 1902.

[8] a) X. Y. Qi, H. Li, J. W. Y. Lam, X. T. Yuan, J. Wei, B. Z. Tang, H. Zhang, *Adv. Mater.* **2012**, DOI: 10.1002/adma.201200026; b) Z. Li, Y. Q. Dong, J. W. Y. Lam, J. X. Sun, A. J. Qin, M. Häußler, Y. P. Dong, H. H. Y. Sung, I. D. Williams, H. S. Kwok, B. Z. Tang, *Adv. Funct. Mater.* **2009**, *19*, 905; c) F. Mahtab, Y. Yu, J. W. Y. Lam, J. Z. Liu, B. Zhang, P. Lu, X. X. Zhang, B. Z. Tang, *Adv. Funct. Mater.* **2011**, *21*, 1733; d) G. Yu, S. W. Yin, Y. Q. Liu, J. S. Chen, X. J. Xu, X. B. Sun, D. G. Ma, X. W. Zhan, Q. Peng, Z. G. Shuai, B. Z. Tang, D. B. Zhu, W. H. Fang, Y. Luo, *J. Am. Chem. Soc.* **2005**, *127*, 6335; e) J. D. Luo, Z. L. Xie, J. W. Y. Lam, L. Cheng, H. Y. Chen, C. F. Qiu, H. S. Kwok, X. W. Zhan, Y. Q. Liu, D. B. Zhu, B. Z. Tang, *Chem. Commun.* **2001**, 1740.

[9] a) Q. Chen, D. Q. Zhang, G. X. Zhang, X. Y. Yang, Y. Feng, Q. H. Fan, D. B. Zhu, *Adv. Funct. Mater.* **2010**, *20*, 3244; b) C. Y. K. Chan, Z. J. Zhao, J. W. Y. Lam, J. Z. Liu, S. M. Chen, P. Lu, F. Mahtab, X. J. Chen, H. H. Y. Sung, H. S. Kwok, Y. G. Ma, I. D. Williams, K. S. Wong, B. Z. Tang, *Adv. Funct. Mater.* **2012**, *22*, 378.

[10] a) H. Tong, Y. Q. Dong, Y. N. Hong, M. Häussler, J. W. Y. Lam, H. H. Y. Sung, X. M. Yu, J. X. Sun, I. D. Williams, H. S. Kwok, B. Z. Tang, *J. Phys. Chem. C* **2007**, *111*, 2287; b) Y. Q. Dong, J. W. Y. Lam, A. J. Qin, Z. Li, J. Z. Sun, H. H. Y. Sung, I. D. Williams, B. Z. Tang, *Chem. Commun.* **2007**, 40; c) M. C. Li, M. Hayashi, S. H. Lin, *J. Phys. Chem. A* **2011**, *115*, 14531.

[11] a) B. K. An, J. Gierschner, S. Y. Park, *Acc. Chem. Res.* **2012**, *45*, 544; b) B. K. An, D. S. Lee, J. S. Lee, Y. S. Park, H. S. Song, S. Y. Park, *J. Am. Chem. Soc.* **2004**, *126*, 10232; c) Y. N. Hong, J. W. Y. Lam, B. Z. Tang, *Chem. Commun.* **2009**, 4332.

[12] a) L. J. Qian, B. Tong, J. B. Shen, J. B. Shi, J. G. Zhi, Y. Q. Dong, F. Yang, Y. P. Dong, J. W. Y. Lam, Y. Liu, B. Z. Tang, *J. Phys. Chem. B* **2009**, *113*, 9098; b) Y. Jin, Y. B. Xu, Y. L. Liu, L. Y. Wang, H. F. Jiang, X. J. Li, D. R. Cao, *Dyes Pigments* **2011**, *90*, 311; c) E. Cariati, V. Lanzeni, E. Tordin, R. Ugo, C. Botta, A. G. Schieroni, A. Sironic, D. Pasinid, *Phys. Chem. Chem. Phys.* **2011**, *13*, 18005.

[13] a) A. Prasanna de Silva, H. Q. Nimal Gunaratne, T. Gunnlaugsson, A. J. M. Huxley, C. P. McCoy, J. T. Rademacher, T. E. Rice, *Chem. Rev.* **1997**, *97*, 1515; b) M. Wang, G. X. Zhang, D. Q. Zhang, D. B. Zhu, B. Z. Tang, *J. Mater. Chem.* **2010**, *20*, 1858.

[14] a) Y. Liu, Y. H. Tang, N. N. Barashkov, I. S. Irgibaeva, J. W. Y. Lam, R. R. Hu, D. Birimzhanova, Y. Yu, B. Z. Tang, *J. Am. Chem. Soc.* **2010**, *132*, 13951; b) Y. Liu, C. M. Deng, L. Tang, A. J. Qin, R. R. Hu, J. Z. Sun, B. Z. Tang, *J. Am. Chem. Soc.* **2011**, *133*, 660; c) S. J. Toal, K. A. Jones, D. Magde, W. C. Trogler, *J. Am. Chem. Soc.* **2005**, *127*, 11661; d) C. Yu, K. H. Y. Chan, K. M. C. Wong, V. W. W. Yam, *Proc. Natl. Acad. Sci. USA.* **2006**, *103*, 19652; e) M. C. L. Yeung, K. M. C. Wong, Y. K. T. Tsang, V. W. W. Yam, *Chem. Commun.* **2010**, *46*, 7709.

[15] a) M. Wang, D. Q. Zhang, G. X. Zhang, Y. L. Tang, S. Wang, D. B. Zhu, *Anal. Chem.* **2008**, *80*, 6443; b) M. Wang, X. G. Gu, G. X. Zhang, D. Q. Zhang, D. B. Zhu, *Anal. Chem.* **2009**, *81*, 4444; c) M. Wang, D. Q. Zhang, G. X. Zhang, D. B. Zhu, *Chem. Commun.*

2008, 4469; d) X. G. Gu, G. X. Zhang, D. Q. Zhang, *Analyst* **2012**, *137*, 365.

[16] a) B. L. Feringa, R. A. van Delden, N. Koumura, E. M. Geertsema, *Chem. Rev.* **2000**, *100*, 1789; b) V. I. Minkin, *Chem. Rev.* **2004**, *104*, 2751; c) S. J. Lim, B. K. An, S. D. Jung, M. A. Chung, S. Y. Park, *Angew. Chem. Int. Ed.* **2004**, *43*, 6346; d) Z. Q. Guo, W. H. Zhu, L. J. Shen, H. Tian, *Angew. Chem. Int. Ed.* **2007**, *46*, 5549.

[17] a) G. Y. Jiang, Y. L. Song, X. F. Guo, D. Q. Zhang, D. B. Zhu, *Adv. Mater.* **2008**, *20*, 2888; b) H. Li, J. X. Wang, H. Lin, L. Xu, W. Xu, R. M. Wang, Y. L. Song, D. B. Zhu, *Adv. Mater.* **2010**, *22*, 1237; c) Y. Q. Wen, J. X. Wang, J. P. Hu, L. Jiang, H. J. Gao, Y. L. Song, D. B. Zhu, *Adv. Mater.* **2006**, *18*, 1983; d) Y. L. Song, D. B. Zhu, *High Density Data Storage: Principle, Technology and Materials*, World Scientific Publishing Co. Pte. Ltd., Singapore **2009**; e) Y. L. Shang, Y. Q. Wen, S. L. Li, S. X. Du, X. B. He, L. Cai, Y. F. Li, L. M. Yang, H. J. Gao, Y. L. Song, *J. Am. Chem. Soc.* **2007**, *129*, 11674.

[18] a) Z. J. Ning, Z. Chen, Q. Zhang, Y. L. Yan, S. X. Qian, Y. Cao, H. Tian, *Adv. Funct. Mater.* **2007**, *17*, 3799; b) G. Q. Zhang, J. W. Lu, M. Sabat, C. L. Fraser, *J. Am. Chem. Soc.* **2010**, *132*, 2160; c) B. K. An, S. K. Kwon, S. D. Jung, S. Y. Park, *J. Am. Chem. Soc.* **2002**, *124*, 14410.

[19] a) J. W. Chung, Y. M. You, H. S. Huh, B. K. An, S. J. Yoon, S. H. Kim, S. W. Lee, S. Y. Park, *J. Am. Chem. Soc.* **2009**, *131*, 8163; b) B. R. Crenshaw, C. Weder, *Chem. Mater.* **2003**, *15*, 4717; c) D. R. T. Roberts, S. J. Holder, *J. Mater. Chem.* **2011**, *21*, 8256.

[20] a) Y. Sagara, T. Kato, *Nat. Chem.* **2009**, *1*, 605; b) T. Mutai, H. Satou, K. Araki, *Nat. Mater.* **2005**, *4*, 685; c) Y. Sagara, S. Yamane, T. Mutai, K. Araki, T. Kato, *Adv. Funct. Mater.* **2009**, *19*, 1869; d) Y. Sagara, T. Kato, *Angew. Chem. Int. Ed.* **2008**, *47*, 5175; e) Y. Sagara, T. Mutai, I. Yoshikawa, K. Araki, *J. Am. Chem. Soc.* **2007**, *129*, 1520.

[21] a) V. N. Kozhevnikov, B. Donnio, D. W. Bruce, *Angew. Chem. Int. Ed.* **2008**, *47*, 6286; b) A. L. Balch, *Angew. Chem. Int. Ed.* **2009**, *48*, 2641; c) T. Lasanta, M. E. Olmos, A. Laguna, J. M. López-de-Luzuriaga, P. Naumov, *J. Am. Chem. Soc.* **2011**, *133*, 16358; d) Y. Lee, R. Eisenberg, *J. Am. Chem. Soc.* **2003**, *125*, 7778; e) S. Perruchas, X. F. Le Goff, S. Maron, I. Maurin, F. Guillen, A. Garcia, T. Gacoin, J. P. Boilot, *J. Am. Chem. Soc.* **2010**, *132*, 10967; f) H. Ito, T. Saito, N. Oshima, N. Kitamura, S. Ishizaka, Y. Hinatsu, M. Wakeshima, M. Kato, K. Tsuge, M. Sawamura, *J. Am. Chem. Soc.* **2008**, *130*, 10044.

[22] Y. S. Wu, J. Li, X. C. Ai, L. M. Fu, J. P. Zhang, Y. Q. Fu, J. J. Zhou, L. Li, Z. S. Bo, *J. Phys. Chem. A* **2007**, *111*, 11473.

[23] Figure S2 in the Supporting Information depicts the absorption spectrum of **1** in THF solution and those of **1a**, **1b** and **1amorphous**. Spectral shifts were observed for **1a**, **1b**, and **1amorphous** compared with the solution spectrum. However, these spectral shifts cannot be simply attributed to the formation of H/J-aggregates because there are no H/J-aggregates within crystals of **1a** and **1b**. It is probable that molecules of **1** adopt different conformations (which can be affected by intermolecular interactions of surrounding molecules) in THF solution, **1a**, **1b**, and **1amorphous**, leading to different absorption spectra in these states.

[24] a) H. M. Senn, W. Thiel, *Angew. Chem. Int. Ed.* **2009**, *48*, 1198; b) O. Acevedo, W. L. Jorgensen, *J. Am. Chem. Soc.* **2006**, *128*, 6141; c) M. Parac, M. Doerr, C. M. Marian, W. Thiel, *J. Comput. Chem.* **2010**, *31*, 90.

[25] X. L. Luo, J. N. Li, C. H. Li, L. P. Heng, Y. Q. Dong, Z. P. Liu, Z. S. Bo, B. Z. Tang, *Adv. Mater.* **2011**, *23*, 3261.

[26] a) S. Varghese, S. Das, *J. Phys. Chem. Lett.* **2011**, *2*, 863; b) N. S. S. Kumar, S. Varghese, C. H. Suresh, N. P. Rath, S. Das, *J. Phys. Chem. C* **2009**, *113*, 11927; c) J. Dong, K. M. Solntsev, L. M. Tolbert, *J. Am. Chem. Soc.* **2009**, *131*, 662; h) N. D. Nguyen, G. Q. Zhang, J. W. Lu, A. E. Shermana, C. L. Fraser, *J. Mater. Chem.* **2011**, *21*, 8409.

[27] L. P. Heng, X. Y. Wang, D. L. Tian, J. Zhai, B. Z. Tang, L. Jiang, *Adv. Mater.* **2010**, *22*, 4716.

[28] This may be interpreted by considering the fact that microrods of **2a** and **3** are wider than those of **1a**, **1b**, and **2b**.

[29] a) H. Yanagi, T. Ohara, T. Morikawa, *Adv. Mater.* **2001**, *13*, 1452; b) H. Wang, F. Li, I. Ravia, B. R. Gao, Y. P. Li, V. Medvedev, H. B. Sun, N. Tessler, Y. G. Ma, *Adv. Funct. Mater.* **2011**, *21*, 3770; c) F. Gao, Q. Liao, Z. Z. Xu, Y. H. Yue, Q. Wang, H. L. Zhang, H. B. Fu, *Angew. Chem. Int. Ed.* **2010**, *49*, 732; d) H. Yanagi, *Chem. Mater.* **2001**, *13*, 4800; e) S. Park, O. H. Kwon, S. Kim, S. Park, M. G. Choi, M. Cha, S. Y. Park, D. J. Jang, *J. Am. Chem. Soc.* **2005**, *127*, 10070; f) D. V. Vezenov, B. T. Mayers, R. S. Conroy, G. M. Whitesides, P. T. Snee, Y. Chan, D. G. Nocera, M. G. Bawendi, *J. Am. Chem. Soc.* **2005**, *127*, 8952.

[30] It was found that microcrystallines of **2a**, **2b**, and **3** started to melt after irradiation with pump laser. Therefore, ASE behaviors were not observed for microcrystalline of **2a**, **2b**, and **3** at room temperature.